Micro and Nanostructures 163 (2022) 107114

Contents lists available at ScienceDirect

Micro and Nanostructures

journal homepage: www.journals.elsevier.com/micro-and-nanostructures

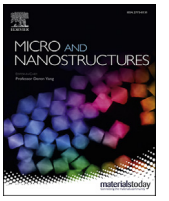

# Double Facet Coated Substrate transmittance model for Cd-doped ZnO thin films

E. Ozugurlu

*Istanbul Technical University, Department of Mathematics, 34469, Maslak, Istanbul, Turkey*

ARTICLE INFO

*Keywords:*
Thin films
ZnO
Extinction coefficient
Refractive index
Urbach energy

ABSTRACT

The sol-gel method was used to grow Cd-doped ZnO ($Zn_{1-x}Cd_xO$) (x = 0.00, 0.01, 0.02, 0.03, 0.04, and 0.05) thin films to analyze the optical properties. A Double Facet Coated Substrate (DFCS) theoretical transmittance model was used to analyze the optical transmittance data and to determine the thickness, absorption loss, extinction coefficient, and refractive index of the thin films. The thicknesses and the refractive indices of the films varied in the range of 240–260 nm and 1.54 to 1.63, respectively. The extinction coefficient follows the dispersion relation of Sellmeier and increases with the Cd concentration while the optical band gap declines as Cd increases from 0.0 to 0.05. On the other hand, 5% of doped Cd films have the highest Urbach energy 85±15 meV. For the structural analysis and determination of surface morphology, we used X-ray diffraction and a scanning electron microscope. For the elemental compositions of the thin films, electron dispersive spectroscopy was used. The study demonstrates the successful application of the DFCS model for accurate determination of refractive index and extinction coefficient which are two essential parameters in the modeling of photolithographic processes in the semiconductor industry.

## 1. Introduction

Optical thin films have been playing an important role in solar cells, medical devices, the auto industry, semiconductors, optoelectronics, biomaterials, data storage, photolithographic semiconductor, and environmental equipment [1–10]. To produce thin films for a specific application, coarseness, thickness, and homogeneity need to be controlled. Various physical and chemical methods can be used to fabricate thin films [11–22]. The sol-gel dip-coating method does not require sophisticated equipment and can be used under non-vacuum/ambient conditions; it is a highly accurate and very convenient method to arrange doping ratios easily. Besides, the good examples of thin films fabricated by the sol-gel technique are in industrial implementations that require big surface areas [3,4,6,8,10,11,15,20,22].

In the last 20 years, researchers have studied the extent to which the optical, electrical, and magnetic properties of zinc oxide are modified when it is doped with B, Cd, Co, Cu, Er, Eu, Mg, Mn, Na, Ni, and Tb [2–4,7,11–14,17–33]. The challenging question is how to determine which element(s) has to be doped into ZnO to decrease the effect of impurities on optical properties, eliminate organic pollutants, improve photocatalytic activity, be useful as buffer layers in solar cells and separate the pollutants from the water. Among all these elements, Cd gives the smallest band gap value in ZnO films. Besides, the electrical conductivity of films can be enhanced by adding Cd into ZnO.

In their review paper, Rajput and Purohit [11] prepared CdO–ZnO thin films with different methods such as sol-gel, sputtering, and

*E-mail addresses:* ozugurlue@itu.edu.tr, eozugurlu@gmail.com.

https://doi.org/10.1016/j.spmi.2021.107114
Received 26 August 2021; Received in revised form 15 November 2021; Accepted 5 December 2021
Available online 8 December 2021

spray pyrolysis techniques on the glass substrate and found that to synthesize CdO–ZnO thin films the sol-gel technique was the best in terms of cost, controllable thickness, desired deposition rate, the semiconducting nature, and polycrystalline nature. They also showed that as Cd concentration increased, the band gap decreased in ZnO films. Yakuphanoglu et al. [22] also used the sol-gel technique and showed that adding Cd into the ZnO film improved the electrical conductivity of the films. In 2019, Kati [3] prepared CdZnO films by using the sol-gel method at different ratios of dopants (CdO:ZnO = 5:5, CdO:ZnO = 6:4, and CdO:ZnO = 8:2) coated on a glass surface and found that the obtained optical band gap $E_g$ values were 2.5 eV, 2.49 eV, and 2.4 eV for the produced CdZnO thin films, respectively. Ilican et al. [9] also deposited CdZnO films by the sol-gel technique onto glass substrates and they observed an important variation in optical properties with increasing Cd concentration. On the other hand, Tarwal et al. [18] used a cheap spray pyrolysis method to study the gas sensing properties of the Cd–ZnO films and they obtained that the cadmium dopant played an important role in fine-tuning the physicochemical and gas sensitivity properties of the ZnO thin films.

The main aim of this study is to determine the optical characteristics such as the thickness, the refractive index, the absorption loss, the extinction coefficient, the Urbach energy, and the band gap energy of $Zn_{1-x}Cd_xO$ (x = 0.00, 0.01, 0.02, 0.03, 0.04, and 0.05) thin films developed by the sol-gel technique considering their optical transmittance data. We use the mathematical model (the Double Facet Coated Substrate (DFCS) transmittance model) proposed by our previous work [20] to calculate the parameters of the Cauchy's dispersion equation of three-terms and two different Lorentzian absorption profiles including the amplitudes of the Lorentzian peaks, the resonance wavelengths, and the corresponding absorption widths.

To attain these results, the equations derived by our previous work [20] were used, and then the experimental transmittance data were fitted numerically to the theoretical model. To obtain the optical band gap numerically from the Tauc plot, the linear regression model was applied to the experimental data and the statistical analysis tools were provided such as the total sum of square (SST), the root-mean-square error (RMSE), the coefficient of determination ($R^2$), the correlation coefficient, and the p-value for F-statistic of the linear fit versus constant model.

## 2. Experimental

### 2.1. Production of thin films

To validate our approach experimentally, the sol-gel technique was used to produce the DFCS samples by covering a soda-lime glass substrate (SLG) with Cd-doped ZnO thin films. We used Zinc acetate dihydrate (ZnAc) and Cadmium acetate tetrahydrate (CdAc) as the originator materials and used methanol (ME) and monoethanolamine (MEA) as thinners and equalizers. We dissolved ZnAc and CdAc in ME with a concentration of 0.25 M and added MEA to the solution as ZnAc and CdAc: MEA ratio is preserved at one-to-one. To achieve a transparent solution, we mixed the ultimate solution continuously with a magnetic stirrer at RT. The standard pH meter was used to measure the pH of the solutions. By adding ME, we controlled the viscidness of the solutions, see the details in Refs. [7,12,21].

To attain excellent thin films, it is crucial to obtain the spotless SLG extremely well. First, we washed SLG with detergent, rinsed it with purified water, sonicated it with 20% sulfuric acid/purified water solution for 5 min, and rinsed it with purified water again. We dried the cleaned substrates under nitrogen flow. All of the contaminants were successfully removed by the cleaning treatment from the surface of the SLG substrate. We dipped the cleaned glass substrates into the Cd-doped ZnO solutions and then we pulled through the vertical furnace at 400 °C. The dilution of the solution withdrawal speed, the number of dipping, and the withdrawal speed controlled the film thickness on the substrate. For the desired thickness, the process was repeated to achieve a dense and uniform film. Then, at 600 °C, to form a crystal structure, we heated the thin films/glass substrates for 30 min.

### 2.2. Characterization of Cd-doped ZnO thin films

The obtained Cd-doped ZnO thin films were characterized using Shimadzu UV mini 1240 UV/Vis/NIR spectrophotometer, Scanning Electron Microscope (SEM) (JEOL, JSM-5910LV). XRD patterns were obtained utilizing the Rigaku Multiflex diffractometer using Cu Kα radiation (λ = 1.5408 Å). As polycrystalline form, the sol-gel technique was used to fabricate $Zn_{1-x}Cd_xO$ (x = 0.00, 0.01, 0.02, 0.03, 0.04, and 0.05) thin films.

## 3. Results and discussion

### 3.1. The equations of transmittance model

The sol-gel dip-coating method, just like Langmuir-Blodgett and chemical bath deposition (CBD) methods, results in a thin film on both sides of the substrate material [20, and the references therein]. Consequently, there are going to be two symmetric thin films on both sides of the substrate as shown in Fig. 1b. In our early study, we named this structure as "Double Facet Coated Substrate" (DFCS), whereas a standard film coated on the substrate was named as "Single Facet Coated Substrate" (SFCS) (Fig. 1a) [20]. The interaction between the light and the DFCS is fundamentally different from the interaction between the light and the SFCS because of the second thin film. Thus, to analyze and characterize the thin films on a substrate, the widely used envelope method (Swanepoel's method) cannot be applied to DFCS systems.

The electric field reflection and transmission coefficients for an air-film-substrate (*afs*) system are respectively given for the equation of the double-facet-coated substrate system of transmittance in Sec.2.1 [20] as:

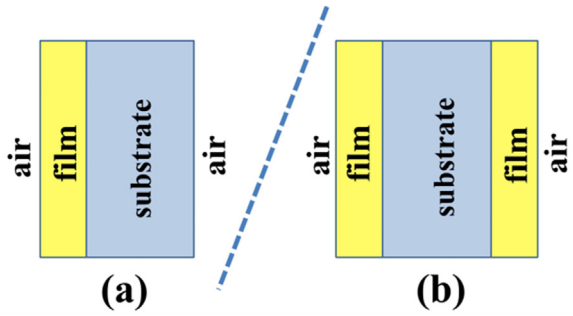


**Fig. 1.** (a) Single facet coated substrate (SFCS), (b) double facet coated substrate (DFCS) [20].

$$r_{afs} = \frac{r_{af} + r_{fs}\exp(i\theta)}{1 + r_{af} r_{fs}\exp(i\theta)} \; and \; t_{afs} = \frac{t_{af} t_{fs} \exp(i\theta/2)}{1 + r_{af} r_{fs} \exp(i\theta)} \tag{1}$$

where $\theta = 4\pi\eta_{film} d_{film}/\lambda$ is the complex phase shift at each round trip through the film of thickness $d_{film}$ at the wavelength $\lambda$, and $\eta_{film}$ is the complex refractive index of the thin film (*af*: air-film, *fs*: film-substrate). However, the experimentally more relevant parameters are the intensity reflectance and transmittance, since they are real numbers and can be measured directly as:

$$R_{afs} = r_{afs} r^{*}_{afs} \; and \; T_{afs} = \frac{n_a}{n_s} t_{afs} t^{*}_{afs} \tag{2}$$

where $n_a$ and $n_s$ are the refractive indices of air and substrate, respectively, and * operator denotes the complex conjugate. Note that these equations assume that the substrate thickness is semi-infinite, and the transmitted light is still inside the substrate medium. If a substrate of finite thickness is considered, then the transmittance formula for $T_{afs}$ transforms into the well-known Swanepoel's formula [20, and the references therein].

As we did in our previous work [20}, we again used a broadband light source having a short coherence length comparable with the thickness of the thin films to measure the transmittance. Therefore, for regions 1 and 3, the acquired phase shift of the electric field due to the film thickness should be considered in the reflectance and transmittance formulae, since these depend on the coherent summation of the multiple reflected electric fields.

However, the thickness of region 2 (i.e. the substrate) is much longer compared to the coherence length of the light source, hence there will not be any interference among the multiple reflected electric fields (i.e. the acquired phase shift through the substrate is irrelevant to the total transmittance). So, the effect of the finite substrate is involved as the summation of the multiple reflected intensities instead of the electric fields. However, the substrate thickness is still taken into consideration in our calculations since it determines the amount of loss the light beam experiences [20].

As shown in Fig. 2, there is an infinite coherent summation inside the first thin film that is phase-dependent, and the transmittance, $T_{afs}$, was given in Eq. (2).

The total transmittance of this DFCS system $T_{system}$ can be calculated by the summation of all these coefficients as stated in Sec. 2.1

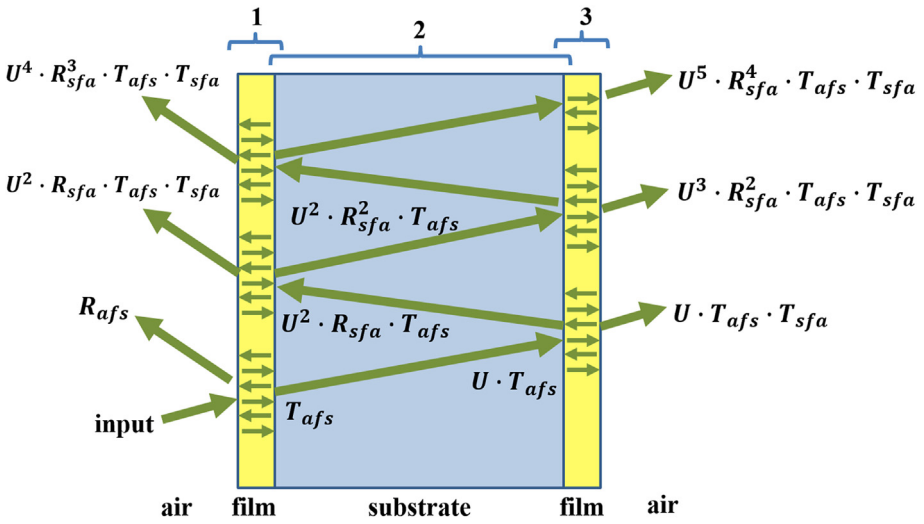


**Fig. 2.** The derivation of the total transmittance formula of the DFCS system [20].

[20]:

$$T_{system} = T_{afs} U T_{sfa} \left(1 + U^2 R_{sfa}^2 + U^4 R_{sfa}^4 + U^6 R_{sfa}^6 + \ldots\right) \tag{3}$$

Using the geometric series expansion formula, provided that $\left|U^2 R_{sfa}^2\right| < 1$, the above equation is simplified as:

$$T_{system} = \frac{T_{afs} T_{sfa} U}{1 - R_{sfa}^2 U^2} \tag{4}$$

where the absorption loss is $U = e^{-\alpha_{sub} \cdot d_{sub}}$, the absorption coefficient of the substrate is $\alpha_{sub}$, $\alpha_{sub} = \frac{4\pi}{\lambda} k_{sub}$, the extinction coefficient of the substrate is $k_{sub}$, and the substrate thickness is $d_{sub}$, the reflection coefficient is $R_{sfa}$, the air-film-substrate (*afs*) transmittance is $T_{afs}$; the substrate-film-air (*sfa*) transmittance is $T_{sfa}$. The reader should note that when $U = 1$ in Equation (4), i.e. a lossless substrate, then the improved Swanepoel's formula is obtained which was reported in our earlier work [16]. Similarly, the total reflectance of the DFCS system $R_{system}$ was also given in Sec.2.1 [20] as

$$R_{system} = R_{afs} + \frac{T_{afs} T_{sfa} R_{sfa} U}{1 - R_{sfa}^2 U^2} \tag{5}$$

To determine $\eta_{film}$, $U$, and $d_{film}$, Equation (4) was used. The dispersion relation of Cauchy of three-term was used to determine the refractive index of the thin film as follows:

$$n_{film} = A + \frac{B}{\lambda^2} + \frac{C}{\lambda^4} \tag{6}$$

Similarly, a wavelength-independent term and two different Lorentzian absorption profiles were used to determine the extinction coefficients of these films as follows:

$$k_{film} = \frac{D}{1 + \left(\frac{\lambda - \lambda_D}{w_D}\right)^2} + \frac{E}{1 + \left(\frac{\lambda - \lambda_E}{w_E}\right)^2} \tag{7}$$

where $D$ and $E$ are the amplitudes of the Lorentzian peaks, $\lambda_D$ and $\lambda_E$ are the resonance wavelengths, $w_D$ and $w_E$ are the absorption widths. The first peak ($D$) explains the absorption near the UV band, while the second peak ($E$) is included to explain the absorption of near-infrared wavelengths. In this analysis, the Kramers-Krönig relation between $\eta_{film}$ and $k_{film}$ was ignored due to the low value of the overall loss at the wavelength range of interest. Rubin introduced the refractive index of the soda-lime-silica glass (SLSG) as [34]:

$$n_{sub} = 1.513 - 3.169 \text{ x } 10^{-3} \lambda^2 + \frac{3.962 \text{ x } 10^{-3}}{\lambda^2} \tag{8}$$

If the film thickness $d_{film} = 0$ or $\eta_{film} = \eta_{air}$, then Equation (4) gives the transmittance of an uncoated substrate. According to our previous calculations [20], the equation of absorption loss $U$ is given as:

$$U = \frac{-T_{as}^2 + \sqrt{T_{as}^4 + 4 R_{as}^2 T_{sub}^2}}{2 R_{as}^2 T_{sub}} \tag{9}$$

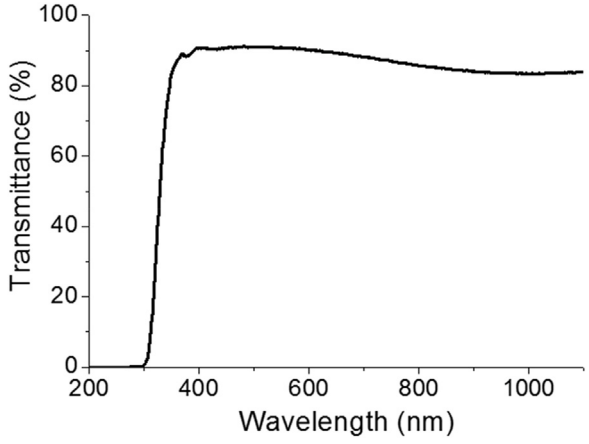


**Fig. 3.** Optical transmittance of uncoated SLSG substrate [20].

where $T_{as}$ is the transmittance of the air-substrate interface, $T_{sub}$ is the experimental transmittance data of the uncoated substrate, and $R_{as}$ is the reflectance of the air-substrate interface. Fig. 3 illustrates $T_{sub}$ vs the wavelength. Once U is calculated, now, to obtain $k_{sub}$ the previously stated equation $U = e^{-\alpha_{sub} \cdot d_{sub}}$ can be used. Using a caliper $d_{sub}$ was found as 1240 μm. If $n_{film}$, $k_{film}$, $n_{sub}$, and $k_{sub}$ are substituted into Equation (4), then $T_{system}$ contains 10 unknown parameters (6 parameters from $k_{film}$, 3 from $n_{film}$, and $d_{film}$).

### 3.2. Structural characterization analysis

Fig. 4 exhibits the X-ray scan of the $Zn_{0.95}Cd_{0.05}O$ thin film on a glass substrate. There is a c-axis oriented (002) peak at $2\theta = 34.50^{\circ}$ of ZnO thin film which indicates a single phase and has a hexagonal wurtzite structure without any Cd-related phase from the XRD pattern.

### 3.3. The morphology characteristics

As illustrated in Fig. 5a–d and 6a - c, the SEM pictures suggest that $Zn_{1-x}Cd_xO$ (x = 0.00, 0.01, 0.02, 0.03, 0.04, and 0.05) thin film

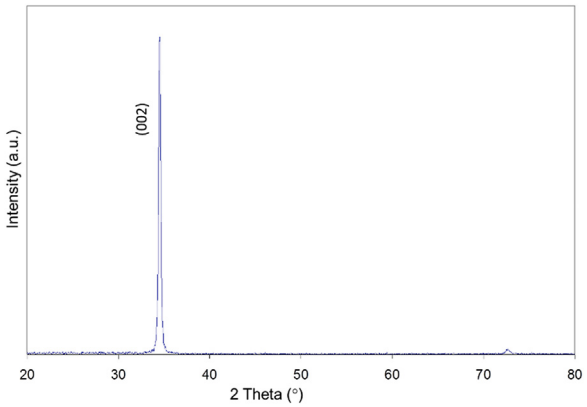


**Fig. 4.** $Zn_{0.95}Cd_{0.05}O$ thin film: XRD pattern with a single phase.

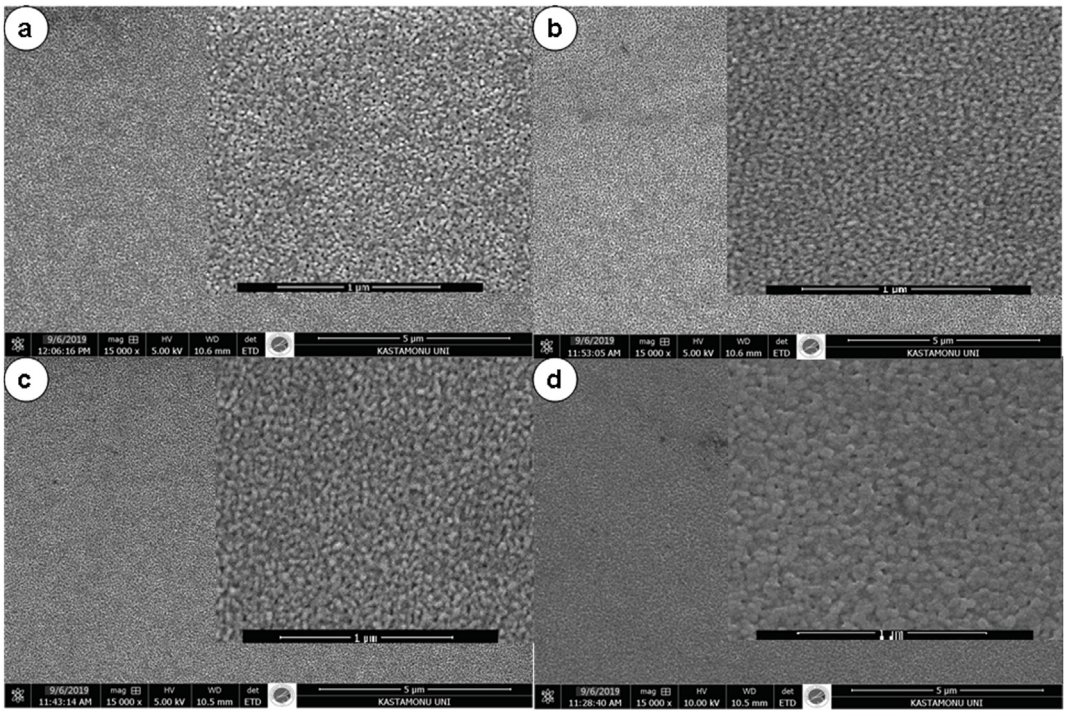


**Fig. 5.** SEM micrographs of thin films a) $Zn_{0.99}Cd_{0.01}O$, b) $Zn_{0.98}Cd_{0.02}O$, c) $Zn_{0.97}Cd_{0.03}O$, and d) $Zn_{0.96}Cd_{0.04}O$.

exhibits similar surfaces covered with tiny pieces. Moreover, all thin films were observed as a crack-free and pinhole-free structure. The thin film thicknesses were measured using SEM to compare our calculated thickness values which are agreed with our results in the range of approximately 250 nm with the relative errors in the range of 0.048–0.068 as illustrated in Fig. 6a (the cross-sectional view of $Zn_{0.95}Cd_{0.05}O$ thin film). The EDS was used to check the elemental composition of the $Zn_{0.95}Cd_{0.05}O$ thin film showing the peaks of zinc, cadmium, and oxygen in Fig. 6d. This showed that the contents of our film compositions were the same as those in the fabrication of thin films.

### 3.4. Calculation of optical band gap energy values for each thin film

The optical band gap energy $E_g$ was calculated by using the relative absorption coefficients and the details of the derivation of the optical band gap $E_g$ can be found in Ref. [32]. By using a linear fitting $y(h\upsilon) = a_1 \times h\upsilon + a_2$ of the absorption edge in the least-squares framework, the slope of the graph of $(F(R_\alpha)\, h\upsilon)^2$ was approximated between 375 and 400 nm, i.e. the following error formula was minimized for $a_1$ and $a_2$,

$$E(A,B) = \sum_{i=1}^{N} \left[a_1 \times (h\upsilon)_i + a_2 - F_i\right]^2 \tag{10}$$

where $N$ is the number of data points and $F_i = (F(R_\alpha)\,(h\upsilon)_i)^2$. Table 1 illustrates $a_1$, $a_2$, $E_g$, and relative error values. $E_g$ is observed in the range of 3.23–3.28 eV which is near the value that Yakuphanoglu et al. found [22].

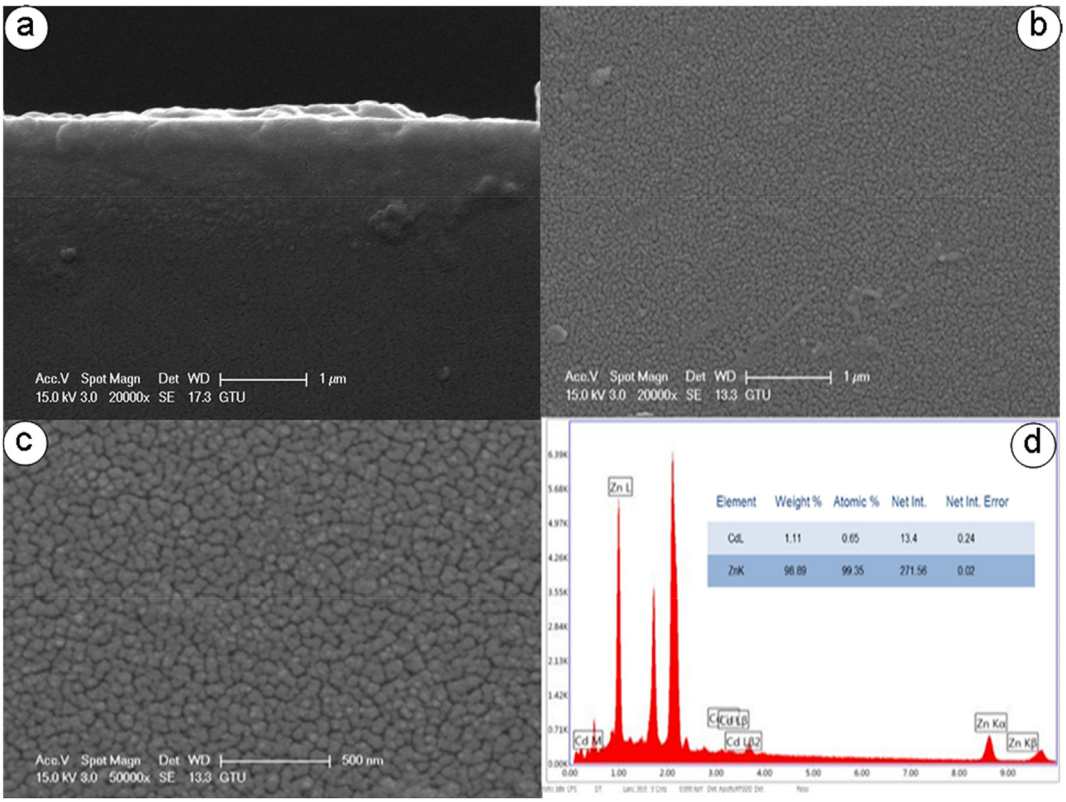


**Fig. 6.** $Zn_{0.95}Cd_{0.05}O$ thin film: a) cross-section, b) and c) SEM images, and d) EDS image.

**Table 1**
Optimized line-fitting parameters $a_1$, $a_2$, and corresponding band gap energies, and relative errors for different Cd doping ratios.

| Cd (%) | $a_1$ | $a_2$ | Band gap (eV) | Relative Error |
|---|---|---|---|---|
| 0 | 15.34 | −50.30 | 3.28 | 0.009 |
| 1 | 13.14 | −42.94 | 3.27 | 0.013 |
| 2 | 12.76 | −41.46 | 3.25 | 0.010 |
| 3 | 13.72 | −44.63 | 3.25 | 0.003 |
| 4 | 13.09 | −42.43 | 3.24 | 0.003 |
| 5 | 12.97 | −41.92 | 3.23 | 0.008 |

For 5% Cd concentration, the band gap energy reached a minimum value of 3.14 eV and it reached a maximum value of 3.28 eV for 0% Cd concentration as illustrated in Table 1 and Fig. 7a-f. The optical band gap of thin films was reduced as Cd concentration increased. This might be because of the replacement of Zn ions with the Cd ions in the ZnO lattice site. The observed band gap energies are in good agreement with the findings of Tarwal et al. [18].

### 3.5. Statistical analysis of the linear regression to find the band gap energy

We used the built-in *fitlm* function of MATLAB to measure the accuracy of our linear regression model as illustrated in Fig. 7a–f and provided the necessary statistics to show how well the model estimates match with the observed responses. We present the statistical analysis tools such as the root mean square error (*RMSE*), the coefficient of determination ($R^2$), the sum of squared total (*SST*), the correlation coefficient, the *p*-value for F-statistic of the linear fit versus constant model in Table 3. However, looking only at the $R^2$ values and the correlation coefficient might be misleading since one has to consider the F-statistic that compares our linear regression model against the constant model. The *p*-value of the model is an indicator of the F-statistic. One can see that the *p* -values were in the order of $10^{-5}$ or smaller as illustrated in Table 2. In all the cases, our model provided a good fit for our data.

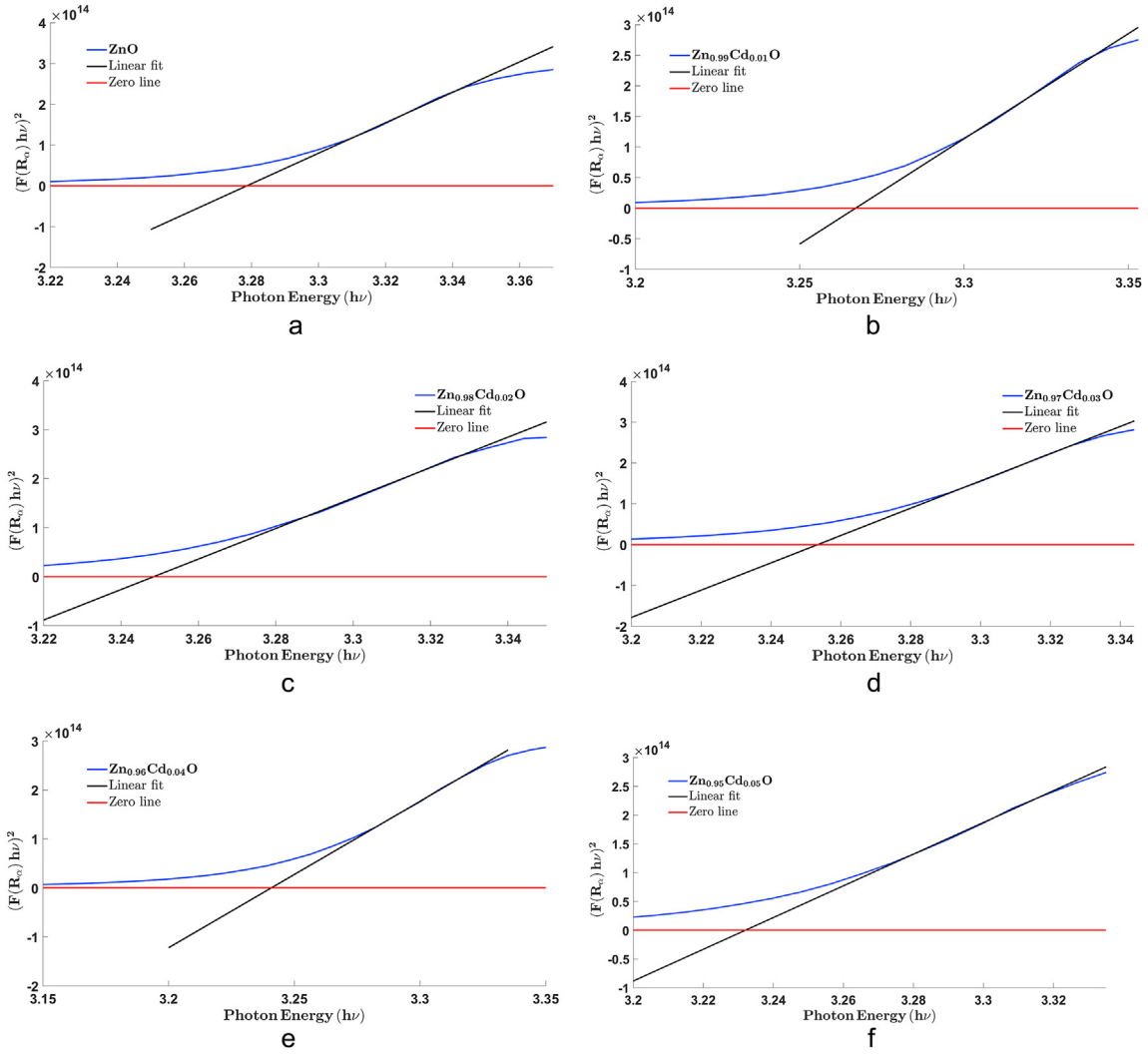


**Fig. 7.** a ZnO thin film: the linear fit (in black) and $(F(R_\alpha)h\nu)^2$ (in blue) (arbitrary unit) vs. photon energy (hν); the optical band gap $E_g = 3.28$ eV. **b.** $Zn_{0.99}Cd_{0.01}O$ thin film: the linear fit (in black) and $(F(R_\alpha)h\nu)^2$ (in blue) (arbitrary unit) vs. photon energy (hν); the optical band gaps $E_g = 3.27$ eV. **c.** $Zn_{0.98}Cd_{0.02}O$ thin film: the linear fit (in black) and $(F(R_\alpha)h\nu)^2$ (in blue) (arbitrary unit) vs. photon energy (hν); the optical band gaps $E_g = 3.25$ eV. **d.** $Zn_{0.97}Cd_{0.03}O$ thin film: the linear fit (in black) and $(F(R_\alpha)h\nu)^2$ (in blue) (arbitrary unit) vs. photon energy (hν); the optical band gaps $E_g = 3.25$ eV. **e.** $Zn_{0.96}Cd_{0.04}O$ thin film: the linear fit (in black) and $(F(R_\alpha)h\nu)^2$ (in blue) (arbitrary unit) vs. photon energy (hν); the optical band gaps $E_g = 3.24$ eV. **f.** $Zn_{0.95}Cd_{0.05}O$ thin film: the linear fit (in black) and $(F(R_\alpha)h\nu)^2$ (in blue) (arbitrary unit) vs. photon energy (hν); the optical band gaps $E_g = 3.23$ eV. .

**Table 2**
The coefficient of determination ($R^2$), the root mean squared error (RMSE), the sum of squared total (SST), the correlation coefficient, and p-value for F-statistic vs. constant model for different Cd doping ratios.

| Cd (%) | $R^2$ | RMSE | SST | Corr. coef. | -value |
|---|---|---|---|---|---|
| 0 | 0.9989 | 0.0084 | 0.1874 | 0.9994 | 0.000016 |
| 1 | 0.9963 | 0.0130 | 0.1379 | 0.9982 | 0.000094 |
| 2 | 0.9985 | 0.0091 | 0.2211 | 0.9992 | 0.000001 |
| 3 | 0.9998 | 0.0031 | 0.1465 | 0.9999 | 0.000001 |
| 4 | 0.9998 | 0.0032 | 0.1321 | 0.9999 | 0.000001 |
| 5 | 0.9984 | 0.0082 | 0.1284 | 0.9992 | 0.000027 |

### 3.6. The Urbach energy

The Urbach law is stated by the following relation between the Urbach energy $E_u$ and the absorption coefficient $\alpha$:

$$\alpha = \alpha_0 e^{h\nu/E_u} \tag{11}$$

where $h\nu$ the photon energy and $\alpha_0$ is a constant [35]. The Urbach energy $E_u$ values can be evaluated by using the following relation [36], and the references therein]:

$$\alpha E_u = \left[\frac{d(\ln \alpha)}{d(h\nu)}\right]^{-1} \tag{12}$$

Fig. 8 displays $\ln \alpha$ versus the photon energy eV ($h\nu$) for $Zn_{1-x}Cd_xO$ films. To approximate $\frac{d(\ln \alpha)}{d(h\nu)}$, we used two finite difference methods (FDMs), namely, 3-point central and 5-point formulas, which are the second and fourth-order accurate approximations, respectively, see the details in Ref. [37]. The application of these FDMs is also listed in Refs. [38,39]. Fig. 9 displays the Urbach energy values $E_u$ and band gap values $E_g$ versus Cd concentration (x) of $Zn_{1-x}Cd_xO$ thin films, listed in Table 3. For undoped ZnO films, Ilican et al. [9] found out that the Urbach energy value $E_u$ was 81 meV. Table 3 illustrates that the Urbach energy value of ZnO thin films increases as cadmium increases. The structural disorder in the $Zn_{1-x}Cd_xO$ films increased as the concentration of Cd increased because of the increase in $E_u$.

### 3.7. Non-linear curve-fitting approach for transmittance data

Since thin films have a huge optical loss below 450 nm, our simulations considered the wavelength range of 450–1100 nm. Fig. 10 exhibits the transmittance data for six different $Zn_{1-x}Cd_xO$ (x = 0.00, 0.01, 0.02, 0.03, 0.04, and 0.05) thin films. The absorption edge of the films exhibited redshifting when we increased the amount of Cd concentration in the ZnO. All films showed the c-axis preferential orientation. Moreover, the optical transparency with visible transmittance >75% was observed in the visible region of 400–600 nm, which shows that the films are transparent in the range of 400–600 nm. It is known that the properties of high transmittance make the films good materials for optical coatings. Moreover, the transmittance decreased as the Cd concentration increased, which indicates that the decrease in the $E_g$ values is due to Cd doping as discussed in Section 3.4. These values are in good agreement with the findings of

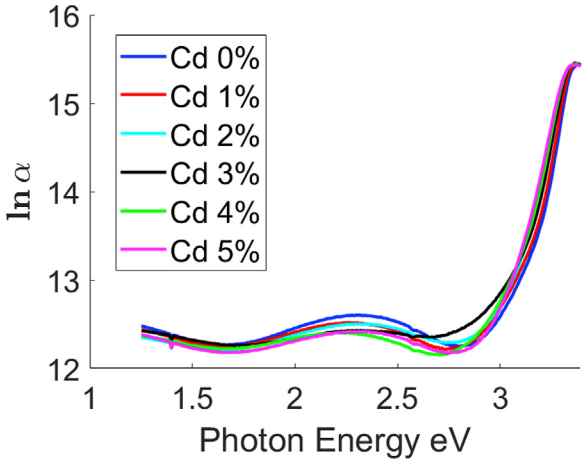


**Fig. 8.** $\ln\alpha$ versus photon energy $h\nu$ (eV) of $Zn_{1-x}Cd_xO$ thin films.

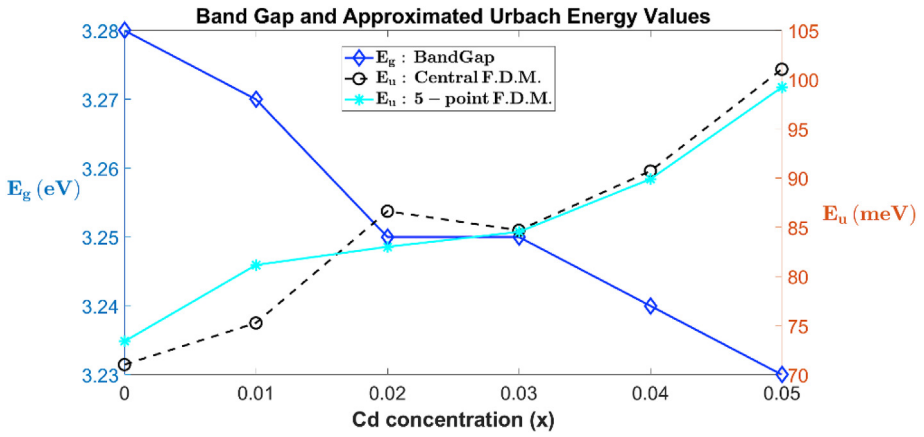


**Fig. 9.** Band gap $E_g$ and Urbach energy ($E_u$) values of $Zn_{1-x}Cd_xO$ thin films vs. Cd concentration (x).

**Table 3**
The Urbach energy $E_u$ values in **meV** using FDMs at or near $E_g$ for the $Zn_{1-x}Cd_xO$ thin films.

| % Cd conc. | 3-point Central FDM | 5-point FDM |
|---|---|---|
| 0 | 71.03 | 73.39 |
| 1 | 75.26 | 81.16 |
| 2 | 86.62 | 83.00 |
| 3 | 84.69 | 84.52 |
| 4 | 90.71 | 89.89 |
| 5 | 101.06 | 99.23 |

The highest value of Urbach energy was obtained for 5% Cd.

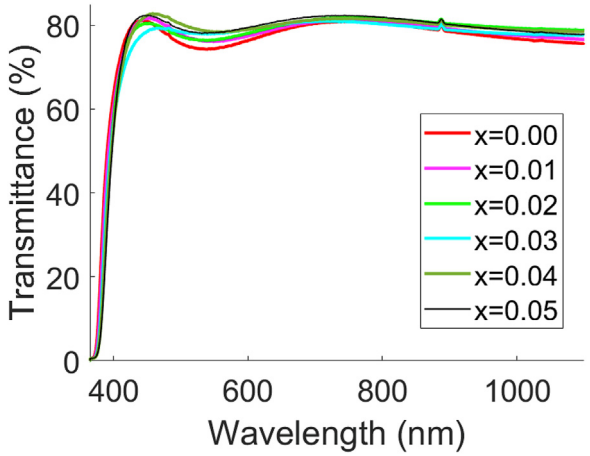


**Fig. 10.** $Zn_{1-x}Cd_xO$ (x = 0.00, 0.01, 0.02, 0.03, 0.04, and 0.05) thin films: experimental transmittance vs. wavelength.

Shohany and Zak [40]. MATLAB was used for the optimization code based on the Nelder-Mead simplex algorithm, i.e. to find the unknowns $\vec{x}$ that minimize the following quantity:

$$\min_{\vec{x}} \sum_{i=1}^{N} T_{system}(\vec{x}, \lambda_i) - T_i^2 \tag{13}$$

where $T_i$ is the transmittance data given input as the observed transmittance data and wavelength data $\lambda$. Here, $N$ is the number of data points, $T_{system}(\vec{x}, \lambda_i)$ was defined in Equation (4), and $\vec{x}$ consists of 10 unknown entries, namely, 3 parameters from $n_{film}$, 6 parameters from $k_{film}$ and $d_{film}$ that need to be optimized. By assuming a wavelength-independent refractive index and loss, the initial values of these

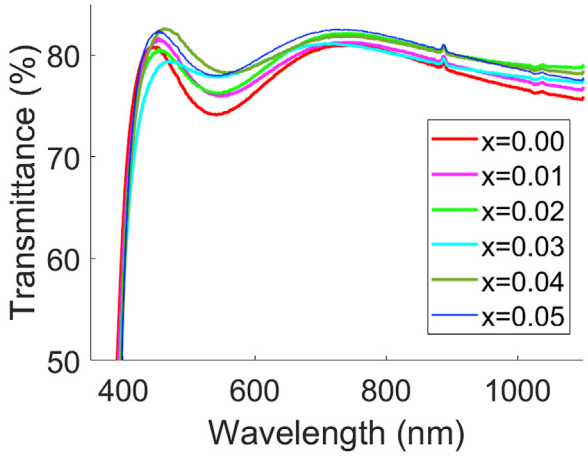


**Fig. 11.** $Zn_{1-x}Cd_xO$ (x = 0.00, 0.01, 0.02, 0.03, 0.04, and 0.05) thin films: theoretical transmittance vs. wavelength.

10 parameters for the curve-fitting problem were determined. Once the optimized 10 unknowns were determined, the curve-fitting models were illustrated in Fig. 11.

We do this by using MATLAB built-in function **lsqcurvefit** e.g.

```
fun = @(x,xdata) (Ttafs(xdata,x,etaa, substrate,sthickness).*
(Ttsfa(xdata,x,etaa, substrate,sthickness) …
.*Uglassloss(xdata, substrate))) …
./(1-Rrafs(xdata,x,etaa, substrate,sthickness).* …
(Rrsfa(xdata,x,etaa, substrate,sthickness) …
.*(Uglassloss(xdata, substrate)).^2));
```

X = **lsqcurvefit** (fun, X0, xdata, ydata, LB, UB) which starts at X0 and finds coefficients X to best fit the nonlinear functions in fun to the data ydata (in the least-squares sense). fun accepts inputs X and xdata and returns a vector of function values F, where F is the same size as ydata, evaluated at X and xdata. Here, LB and UB are the lower and upper bounds, respectively for X.

X = **lsqcurvefit** (fun, X0, xdata, ydata, LB, UB) defines a set of lower and upper bounds on the design variables, X, so that the solution is in the range LB≤X ≤ UB.

The experimental transmittance data and the theoretical curve fittings were plotted versus the wavelength with their zoomed graphs in Fig. 12 a-c. As mentioned earlier in our previous work [20], there were small peaks at 950 nm on all plots in Fig. 12 a-c, the substrate was the reason for this. Besides, our model used the experimental data to derive the substrate loss.

The optimum values of 10 unknowns were obtained by the curve-fitting model using the Nelder-Mead simplex algorithm as listed in Table 4. Moreover, the following formula

$$\sqrt{\sum\left(\frac{|Experimental\ Data - Curve\ Fitting|}{|Experimental\ Data|}\right)^2} \tag{14}$$

was used for the relative error of each fitting and illustrated in Table 4.

### 3.8. Dispersion relation and extinction coefficient

Fig. 13 exhibits the dispersion relation (Equation (6)) for each thin film. Fig. 13 indicates that the range of average refractive index values is between 1.508 and 1.785. These values are in good agreement with the findings of Ziabari et al. [23]. After the wavelength $\lambda >$ 650 nm, the high refractive index values appear for 10% Cd concentration. Besides, Fig. 14 illustrates an increasing trend of the extinction coefficient $k_{film}$ given by Equation (7) for each film using the values from Table 4 as Cd concentration increases and this is also confirmed by Sellmeier's dispersion relation [10].

## 4. Conclusion

The sol-gel technique was used to fabricate c-axis oriented (002) hexagonal wurtzite $Zn_{1-x}Cd_xO$ (x = 0.00, 0.01, 0.02, 0.03, 0.04, and 0.05) thin films with a single-phase, and DFCS model was used to determine their optical properties [20]. We found that the thicknesses of the films were in the range of 240–260 nm which were close to the actual value of 250 nm. The refractive index was in the range of 1.54–1.63 and had a pattern of a decreasing function approaching 1.5. The optical band gap energy values of the Cd-doped ZnO thin

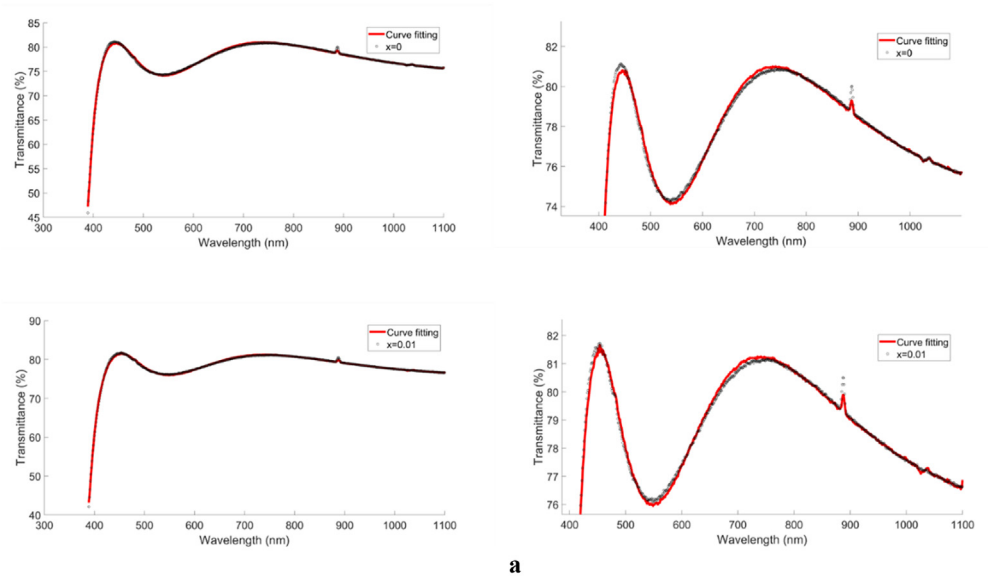


a

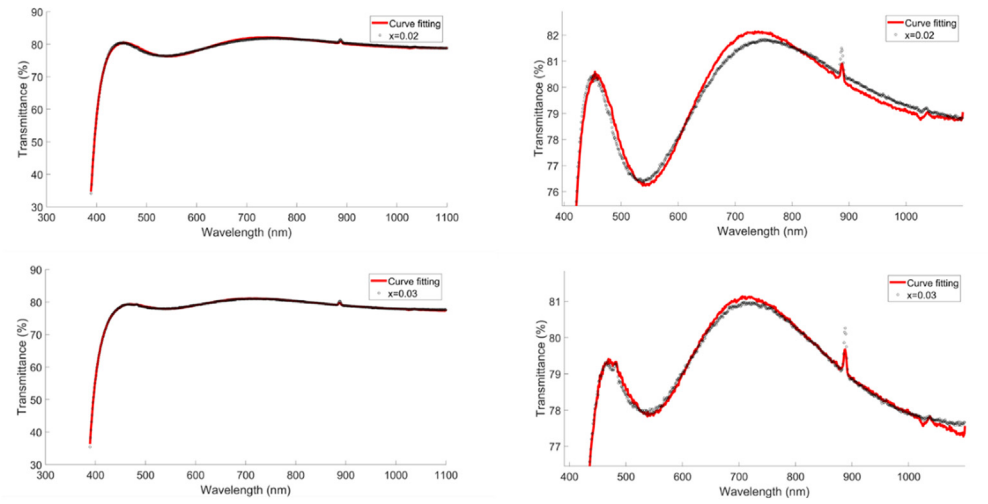


b

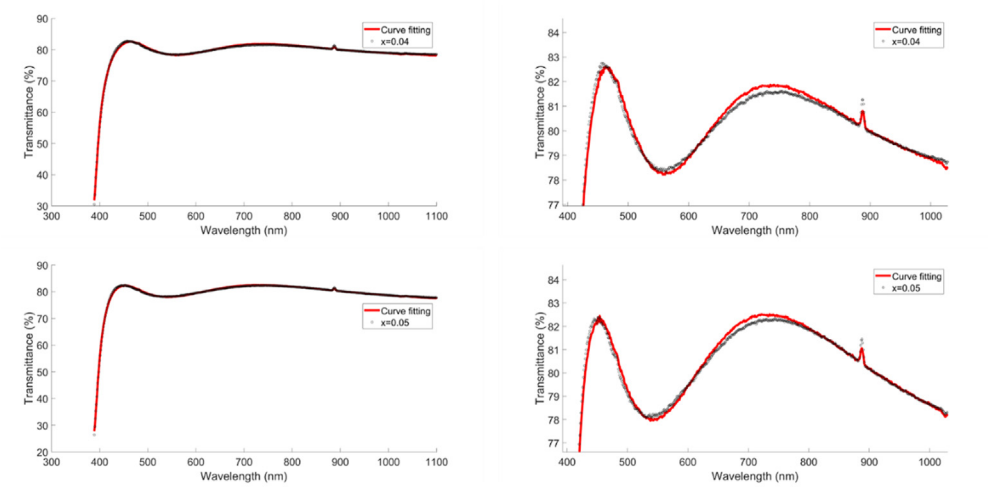


c

*(caption on next page)*

**Fig. 12.** a. $Zn_{1-x}Cd_xO$ thin films: Top: x = 0.0, Bottom: x = 0.01 for experimental transmittance data (in black), and the theoretical curve fittings (in red) vs. wavelength (on the left column), and the zoomed one on the right column. **b.** $Zn_{1-x}Cd_xO$ thin films: Top: x = 0.02, Bottom: x = 0.03 for experimental transmittance data (in black), and the theoretical curve fittings (in red) vs. wavelength (on the left column), and the zoomed one on the right column. **c.** $Zn_{1-x}Cd_xO$ thin films: Top: x = 0.04, Bottom: x = 0.05 for experimental transmittance data (in black), and the theoretical curve fittings (in red) vs. wavelength (on the left column), and the zoomed one on the right column. .

**Table 4**
$Zn_{1-x}Cd_xO$ thin films (x = 0.00, 0.01, 0.02, 0.03, 0.04, and 0.05): optimized curve-fitting model parameters and the relative errors.

| *x* | 0.00 | 0.01 | 0.02 | 0.03 | 0.04 | 0.05 |
|---|---|---|---|---|---|---|
| *A* | 1.51 | 1.50 | 1.46 | 1.43 | 1.47 | 1.53 |
| *B* | 0.08 | 0.07 | 0.10 | 0.10 | 0.08 | 0.05 |
| *C* | −0.01 | 0.00 | −0.01 | −0.01 | −0.01 | 0.00 |
| *D* | 0.33 | 0.31 | 0.50 | 0.28 | 0.31 | 0.23 |
| *E* | 0.10 | 0.10 | 0.04 | 0.13 | 0.09 | 0.14 |
| $w_D(\mu m)$ | 0.39 | 0.38 | 0.38 | 0.37 | 0.38 | 0.39 |
| $w_E(\mu m)$ | 0.01 | 0.01 | 0.01 | 0.01 | 0.01 | 0.01 |
| $\lambda_D(\mu m)$ | 0.03 | 0.04 | 0.07 | 0.18 | 0.06 | 0.07 |
| $\lambda_E(\mu m)$ | 1.75 | 1.75 | 1.75 | 1.75 | 1.75 | 1.75 |
| *F.T.* $(\mu m)$ | 0.24 | 0.25 | 0.25 | 0.26 | 0.26 | 0.25 |
| *S.T.* $(\mu m)$ | 1240 | 1240 | 1240 | 1240 | 1240 | 1240 |
| *Rel. Error* | 0.0024 | 0.0021 | 0.0035 | 0.0016 | 0.0030 | 0.0027 |

where F.T., S.T., and Rel. Error stand for film and substrate thicknesses, and relative error, respectively.

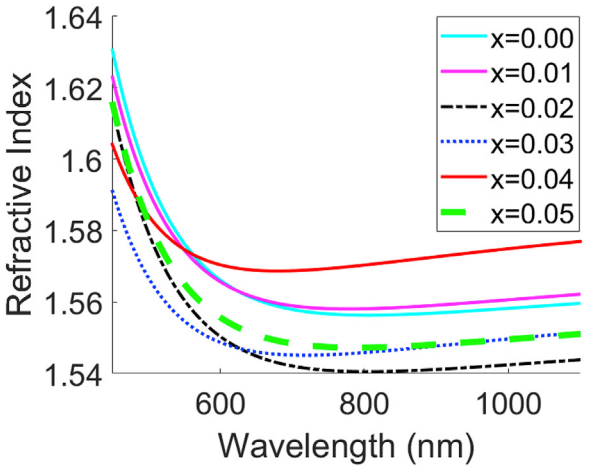


**Fig. 13.** $Zn_{1-x}Cd_xO$ (x = 0.00, 0.01, 0.02, 0.03, 0.04, and 0.05) thin films: refractive index vs. wavelength.

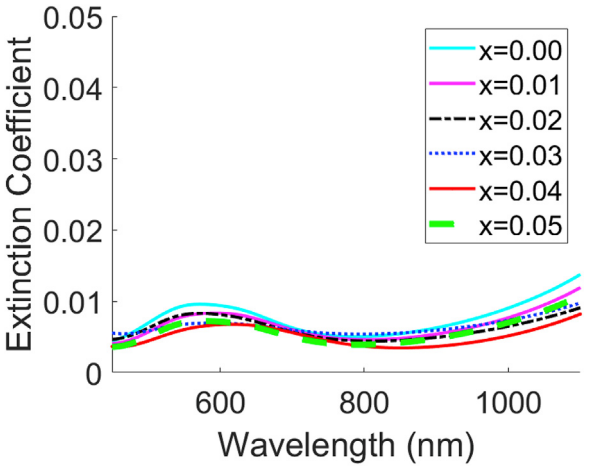


**Fig. 14.** $Zn_{1-x}Cd_xO$ (x = 0.00, 0.01, 0.02, 0.03, 0.04, and 0.05) thin films: extinction coefficient vs. wavelength.

films were observed in the range of 3.23–3.28 eV where the minimum occurred at 5% Cd concentration with a value of 3.23 eV and the maximum occurred at 0% Cd concentration with a value of 3.28 eV. Statistical analysis showed that our linear regression model for obtaining the band gap was very good, where the $p$ -values were in the order of $10^{-5}$ or smaller. The highest value of Urbach energy was found for 5% Cd concentration. These low optical band gap thin films may be useful for optoelectronic applications. Besides, the refractive index and extinction coefficient play important roles in the modeling of photolithographic processes in the semiconductor industry.

## Data availability statement

No new data were created or analyzed in this study.

## Declaration of competing interest

The authors declare that they have no known competing financial interests or personal relationships that could have appeared to influence the work reported in this paper.

## Acknowledgements

The author is grateful for the suggestions and comments made by the referees and thanks to the members of the lab of Bahcesehir University - Istanbul, Turkey and Sarper Ozharar (NEC Inc., New Jersey, USA) for their constructive comments and for providing XRD, EDX, and SEM data.

## References

[1] C. Portesia, L. Lolli, E. Taralli, M. Rajteri, E. Monticone, E-beam evaporated ZnO thin films: fabrication and characterization as UV detector, Eur. Phys. J. Plus 130 (2015) 45.
[2] D.W. Ma, Z.Z. Ye, J.Y. Huang, L.P. Zhu, B.H. Zhao, J.H. He, Effect of post-annealing treatments on the properties of $Zn_{1-x}Cd_xO$ films on glass substrates, Mater. Sci. Eng. B 111 (1) (2004) 250–255.
[3] N. Kati, Controlling of optical bandgap of the CdO films by zinc oxide, Mater. Sci.-Poland 37 (1) (2019) 136–141.
[4] R.A. Zargar, A.H. Shah, M. Arora, Crystallographic, spectroscopic and electrical study of ZnO:CdO nanocomposite-coated films for photovoltaic applications, Arabian J. Sci. Eng. 44 (2019) 6631–6636.
[5] K. Karthik, S. Dhanuskodi, C. Gobinath, et al., Photocatalytic and antibacterial activities of hydrothermally prepared CdO nanoparticles, J. Mater. Sci. Mater. Electron. 28 (2017) 11420–11429.
[6] A. Nivetha, S. Devi Mangala, I. Prabha, Fascinating physic-chemical properties and resourceful applications of selected cadmium nanomaterials, J. Inorg. Organomet. Polym. 29 (2019) 1423–1438.
[7] D. Akcan, A. Gungor, L. Arda, Structural and optical properties of Na-doped ZnO films, J. Mol. Struct. 1161 (2018) 299–305.
[8] A. Amri, Z.T. Jiang, T. Pryor, C.Y. Yin, Z. Xie, N. Mondinos, Optical and mechanical characterization of novel cobalt-based metal oxide thin films synthesized using sol-gel dip-coating method, Surf. Coating. Technol. 207 (2012) 367–374.
[9] S. Ilican, Y. Caglar, M. Caglar, M. Kundakci, A. Ates, Photovoltaic solar cell properties of $Cd_xZn_{1-x}O$ films prepared by sol-gel method, Int. J. Hydrogen Energy 34 (2009) 5201.
[10] Z.N. Kayani, M. Iqbal, S. Riaz, R. Zia, S. Naseem, Fabrication and properties of zinc oxide thin film prepared by sol-gel dip-coating method, Mater. Sci. 33 (3) (2015) 515–520.
[11] J.K. Rajput, L.P. Purohit, Comparative study of synthesis of CdO-ZnO nanocomposite thin films by different methods: a review, Nanosci. Technol. 3 (1) (2016) 1–5.
[12] E. Asikuzun, O. Ozturk, L. Arda, C. Terzioglu, Preparation, growth, and characterization of nonvacuum Cu-doped ZnO thin films, J. Mol. Struct. 1165 (2018) 1–7.
[13] J.W. Mares, F.R. Ruhge, A.V. Thompson, et al., Optical and morphological properties of MBE grown wurtzite $Cd_xZn_{1-x}O$ thin films, Opt. Mater. 30 (2) (2007) 346–350.
[14] S. Ghosh, U.M.K. Kumar, B.N.S. Bhaktha, Heat-treatment controlled structural and optical properties of sol-gel fabricated Eu: ZnO thin films, Opt. Mater. 64 (2017) 288–294.
[15] R.S. Singh, S. Bhushan, A.K. Singh, S.R. Deo, Characterization and optical properties of CdSe nano-crystalline thin films, Dig. J. Nanomater. Biostruct. 6 (2) (2011) 403–412.
[16] S. Ozharar, D. Akcan, L. Arda, Determination of the refractive index and the thickness of double side coated thin films, J. Optoelectron. Adv. Mater. 18 (1–2) (2016) 65–69.
[17] L. Arda, The effects of Tb doped ZnO nanorod: an EPR study, J. Magn. Magn. 475 (2019) 493–501.
[18] N.L. Tarwal, A.R. Patil, N.S. Harale, A.V. Rajgure, S.S. Suryavanshi, W.R. Bae, et al., Gas sensing performance of the spray deposited Cd-ZnO thin films, J. Alloys Compd. 598 (2014) 282–288.
[19] M. Tosun, L. Arda, Effect of temperature and film thickness on structural and mechanical properties of c-axis oriented $Zn_{0.95}Mg_{0.05}O$ thin films, Ceram. Int. 45 (13) (2019) 16234–16243.
[20] D. Akcan, S. Ozharar, E. Ozugurlu, L. Arda, The effects of Co/Cu Co-doped ZnO thin films: an optical study, J. Alloys Compd. 797 (2019) 253–261.
[21] E. Asikuzun, O. Ozturk, L. Arda, C. Terzioglu, Microstructural and electrical characterizations of transparent Er-doped ZnO nano-thin films prepared by sol-gel process, J. Mater. Sci. Mater. Electron. 28 (2017) 14314–14322.
[22] F. Yakuphanoglu, S. Ilican, M. Caglar, Y. Caglar, Microstructure and electro-optical properties of sol-gel derived Cd-doped ZnO films, Appl. Surf. Sci. 255 (2009) 4491.
[23] A. Ziabari Abdolahzadeh, F.E. Ghodsi, Optoelectronic studies of sol-gel derived nanostructured CdO–ZnO composite films, J. Alloys Compd. 509 (35) (2011) 8748–8755.
[24] I.P. Duru, E. Ozugurlu, L. Arda, A first-principles study of Mg/Ni induced magnetic properties of Zn0.95-xMgxNi0.05O, J. Magn. Magn. 504 (2020).
[25] I.P. Duru, E. Ozugurlu, L. Arda, A first-principles study of magnetic properties of $Zn_{0.94}Mg_{0.01}Mn_{0.05}O$, Mater. Res. Express 6 (12) (2019).
[26] I.P. Duru, E. Ozugurlu, L. Arda, Size effect on magnetic properties of $Zn_{0.95-x}Mg_xNi_{0.05}O$ nanoparticles by Monte Carlo simulation, Ceram. Int. 45 (5) (2019) 5259–5265.
[27] E. Ozugurlu, Cd-doped ZnO nanoparticles: an experimental and first-principles DFT studies, J. Alloys Compd. (2021) 861.
[28] E. Ozugurlu, Estimation of structural and optical parameters of (Mg, B) co-doped ZnO nanoparticles, Gazi Univ. J. Sci. 34 (2) (2021) 529–548.

[29] A. Guler, L. Arda, N. Dogan, C. Boyraz, E. Ozugurlu, The annealing effect on microstructure and ESR properties of (Cu/Ni) co-doped ZnO nanoparticles, Ceram. Int. 45 (2) (2019) 1737–1745.
[30] S.D. Senol, C. Boyraz, E. Ozugurlu, A. Gungor, L. Arda, Band gap engineering of Mg doped ZnO nanorods prepared by a hydrothermal method, Cryst. Res. Technol. 54 (3) (2019).
[31] S.D. Senol, B. Yalcin, E. Ozugurlu, L. Arda, Structure, microstructure, optical and photocatalytic properties of Mn-doped ZnO nanoparticles, Mater. Res. Express 7 (1) (2020).
[32] S.D. Senol, E. Ozugurlu, L. Arda, The effect of cobalt and boron on the structural, microstructural, and optoelectronic properties of ZnO nanoparticles, Ceram. Int. 46 (6) (2020) 7033–7044.
[33] M. Tosun, S.D. Senol, L. Arda, Effect of Mn/Cu co-doping on the structural, optical and photocatalytic properties of ZnO nanorods, in: J. Molecular Structure, 7th Inorganic Chemistry Congress, 2020, p. 1212. Corum, Turkey.
[34] M. Rubin, Optical properties of soda-lime silica glasses, Sol. Energy Mater. 12 (1985) 275–288.
[35] H. He, F. Zhuge, Z. Ye, L. Zhu, F. Wang, B. Zhao, J. Huang, Strain and its effect on optical properties of Al-N codoped ZnO films, J. Appl. Phys. 99 (2006), 023503.
[36] R. Vettumperumal, S. Kalyanaraman, B. Santoshkumar, R. Thangavel, Estimation of electron-phonon coupling and Urbach energy in group-I elements doped ZnO nanoparticles and thin films by sol-gel method, Mater. Res. Bull. 77 (2016) 101–110.
[37] R.J. LeVeque, Finite Difference Methods for Ordinary and Partial Differential Equations: Steady-State and Time-dependent Problems, vol. 98, SIAM, 2007.
[38] E. Ozugurlu, A note on the numerical approach for the reaction-diffusion problem with a free boundary condition, ANZIAM 51 (3) (2010) 317–330.
[39] E. Ozugurlu, A note on the numerical approach for the reaction-diffusion problem to model the density of the tumor growth dynamics, Comput. Math. Appl. 69 (12) (2015) 1504–1517.
[40] B.G. Shohany, A.K. Zak, Doped ZnO nanostructures with selected elements - structural, morphology and optical properties: a review, Ceram. Int. 46 (2020) 5507–5520.